Infrared Photodissociation Spectroscopy of $Al^+(CH_3OH)_n$ ($n = 1-4$)

Ari Furuya,[†] Mamoru Tsuruta,[†] Fuminori Misaizu,*[,†] Koichi Ohno,[†] Yoshiya Inokuchi,[‡,§] Ken Judai,[‡] and Nobuyuki Nishi*[,‡]

Department of Chemistry, Graduate School of Science, Tohoku University, Aramaki, Aoba-ku, Sendai 980-8578, Japan, Institute for Molecular Science, Nishigo-naka 38, Myodaiji, Okazaki 444-8585, Japan, and Department of Chemistry, Graduate School of Science, Hiroshima University, Higashi-Hiroshima 739-8526, Japan

Received: November 16, 2006; In Final Form: May 12, 2007

Infrared photodissociation spectra of $Al^+(CH_3OH)_n$ ($n = 1-4$) and $Al^+(CH_3OH)_n-Ar$ ($n = 1-3$) were measured in the OH stretching region, 3000−3800 cm^{-1}. For $n = 1$ and 2, sharp absorption bands were observed in the free OH stretching region, all of which were well reproduced by the spectra calculated for the solvated-type geometry with no hydrogen bond. For $n = 3$ and 4, there were broad vibrational bands in the energy region of hydrogen-bonded OH stretching vibrations, 3000−3500 cm^{-1}. Energies of possible isomers for the $Al^+(CH_3OH)_{3,4}$ ions with hydrogen bonds were calculated in order to assign these bands. It was found that the third and fourth methanol molecules form hydrogen bonds with methanol molecules in the first solvation shell, rather than a direct bonding with the Al^+ ion. For the $Al^+(CH_3OH)_n$ clusters with $n = 1-4$, we obtained no evidence of the insertion reaction, which occurs in $Al^+(H_2O)_n$. One possible explanation of the difference between these two systems is that the potential energy barriers between the solvated and inserted isomers in the $Al^+(CH_3OH)_n$ system is too high to form the inserted-type isomers.

1. Introduction

Gas-phase clusters have long been a subject of interest, because these can be regarded as microscopic models of a condensed phase, and also because there may still remain unveiled novel species in this phase. However, it was difficult to obtain detailed information on the structures of the clusters until recently, except for some specific systems. This difficulty was caused by the relatively low concentration of the clusters, which made the application of conventional spectroscopic techniques impossible. Recently, photodissociation spectroscopy using infrared (IR) light has been widely applied in order to investigate structures of cluster ions such as molecular cluster ions,[1−5] metal cluster ions,[6] and metal-molecule binary cluster ions[7−9] because of the development of strong IR light sources, such as IR optical parametric oscillator (OPO) systems and free electron lasers.[8,10] In particular, cluster ions including water molecules such as protonated water clusters ($H^+(H_2O)_n$) and hydroxide ion−water clusters ($OH^-(H_2O)_n$) have been extensively studied as microscopic models of condensed phase because of their fundamental importance in aqueous chemistry and biochemistry.[1−5] On the other hand, binary clusters consisting of a metal atom (or its ion) and some polar molecules have also been examined for a large number of systems in order to elucidate solvation structures in the clusters.[7−9] Along with the stepwise solvation structures, intracluster reactions were also reported in metal−molecule binary clusters such as an intracluster cyclization reaction in a $Ni^+-C_2H_2$ system.[11] More recently, Inokuchi et al. reported the results of IR photodissociation spectroscopy of a hydrated aluminum monocation, $Al^+(H_2O)_n$ ($n = 1$ and 2), in which an insertion reaction of Al^+ into an OH bond of a water molecule was found to occur in $Al^+(H_2O)_n$.[12] This insertion reaction proceeds in the cluster size of $n = 2$, whereas a solvated-type isomer having a direct bond between Al^+ and an O atom of water (Al^+-OH_2) was formed at $n = 1$. For the $n = 1$ ion, the OH-inserted isomer was reported to be a metastable structure, which was 49.36 kJ/mol higher in energy than the solvated-type isomer.[13] On the other hand, the inserted-type isomer was calculated to be more stable than the solvated-type isomer for $n = 2$. Thus the experimentally observed isomers in $Al^+(H_2O)_n$ were explained by their relative stability. The insertion reaction of an Al^+ ion into an NH bond of an NH_3 molecule were also reported in $Al^+(NH_3)_n$, which can be explained by their energetics again.[14] On the basis of these recent examinations, it is highly interesting to examine whether the Al^+ ion can insert into CO or OH bonds of a methanol molecule. In this study, geometrical structures and a possibility of insertion reactions in the cluster ions with an aluminum monocation and methanol molecules $Al^+(CH_3OH)_n$ have been studied by using IR photodissociation spectroscopy along with theoretical calculation.

2. Experiment

Details of the experimental setup have been described elsewhere.[12] The apparatus consists of an ion-guide mass spectrometer with two quadrupole mass filters. Cluster ions containing an aluminum monocation (Al^+) and methanol molecules (CH_3OH) were produced in a pickup source with a combination of laser vaporization and supersonic expansion. A rotating and translating Al rod (6 mm diameter), which was mounted 10 mm downstream from a pulsed valve (General Valve, series 9, orifice diameter 0.8 mm), was irradiated with the second harmonic of a Nd:YAG laser (Spectra Physics, INDI-50) to produce the Al^+ ion. Synchronized with the generation

* To whom correspondence should be addressed. E-mail: misaizu@qpcrkk.chem.tohoku.ac.jp; nishi@ims.ac.jp.
[†] Tohoku University.
[‡] Institute for Molecular Science.
[§] Hiroshima University.

10.1021/jp067622c CCC: $37.00
Published on Web 06/15/2007

of the Al^+ ion, methanol vapor seeded in argon buffer gas was expanded from the pulsed valve to form methanol clusters. The mixture gas of methanol and argon was obtained by passing Ar gas through a reservoir containing liquid methanol. A mixing ratio was determined by optimizing the ion intensity of a given size. Cluster ions containing Al^+ and CH_3OH were then produced by collisions between the metal ion and the molecular clusters. After the collimation with a conical skimmer, the produced ion beam was introduced into the first quadrupole mass filter with a 50 eV kinetic energy.

After the mass isolation of the parent cluster ions with the first quadrupole mass filter, the selected ions were deflected at a right angle in the ion bender, and they were introduced into the quadrupole ion guide operated in RF-only mode. These parent ions were then irradiated with a counterpropagating IR light, which induced vibrational excitation of the ions when a frequency of the light was matched with a vibrational frequency. Vibrational excitation of the parent ions results in a fragmentation of the ions after the intra- and intermolecular vibrational energy relaxation. Resultant fragment ions were mass-analyzed by a second quadrupole mass filter and detected by a secondary electron multiplier tube. Ion signals from the detector were stored in a digital storage oscilloscope (LeCroy, 9314A) and were typically averaged over 200 laser shots.

An OPO system (Continuum, Mirage 3000) pumped by an injection-seeded Nd:YAG laser (Continuum, Powerlite 9010) was used as a tunable IR light source. The output energy and the line width are typically 1−2 mJ/pulse and ∼1 cm^{-1}, respectively. In order to prevent saturation and nonresonant multiphoton processes, the IR light was loosely focused before entering the vacuum chamber. The frequency of the IR light was calibrated by a commercial wavemeter (Burleigh, WA-4500). Photofragment ion yield was normalized by the intensity of the IR light as well as by the parent ion signal, to minimize fluctuations with time and to improve the signal-to-noise ratio of the dissociation spectra. Photodissociation spectra were obtained by plotting fragment ion intensity as a function of photon energy.

A messenger technique with an Ar atom is used to form cold cluster ions as well as enhance the dissociation probability after photon absorption because the binding energy of an Ar atom is comparatively small. For example, the bond dissociation energy of Al^+−Ar in the ground state was determined to be 1025 cm^{-1},[15] which is much smaller than the energy of an OH stretching vibration (3000−3800 cm^{-1}). Thus, the dissociation of the Ar atom from $Al^+(CH_3OH)_n$−Ar to produce bare $Al^+(CH_3OH)_n$ was easily caused by the absorption of an IR photon corresponding to the OH stretching vibration. Therefore, we can obtain enhanced signals from a parent ion of $Al^+(CH_3OH)_n$−Ar with small internal energy.

3. Calculation

Geometrical structures of $Al^+(CH_3OH)_n$ (n = 1−4) and $Al^+(CH_3OH)_n$−Ar (n = 1−3) cluster ions were optimized by a density functional theory (DFT) calculation with the Becke−3−Lee−Yang−Parr (B3LYP) functional[16] of the Gaussian 03 package[17] with a 6-31+G(d) basis set. Harmonic vibrational frequencies were also calculated at the same level of theory in order to ensure that equilibrium structures were obtained in the geometry optimization. Energies of the calculated geometries are corrected by zero-point vibrational energy by using the harmonic frequencies. Theoretical vibrational spectra were obtained by the calculated frequencies and IR intensities with a frequency-scaling factor of 0.9654, which was used in a previous IR photodissociation study on $Mg^+(H_2O)_n$ and $Al^+(H_2O)_n$.[18] The basis set superposition error (BSSE) was not included in all energies presented here because calculated results with BSSE correction were essentially the same as those obtained without the correction for n = 1.

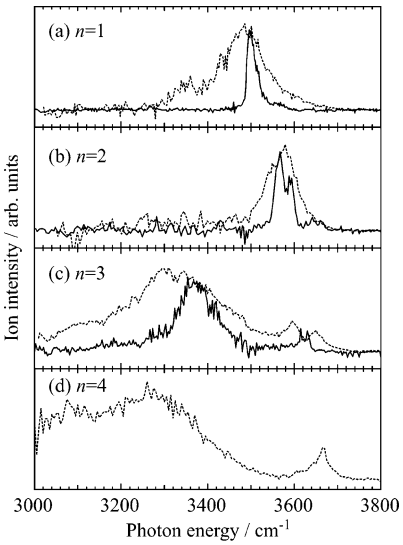

Figure 1. IR photodissociation spectra of bare $Al^+(CH_3OH)_n$ (n = 1−4) (dashed lines) and $Al^+(CH_3OH)_n$−Ar (n = 1−3) (solid lines) obtained by monitoring $Al^+(CH_3OH)_{n-1}$ and $Al^+(CH_3OH)_n$ ions, respectively, as a function of the frequency of the dissociation IR light. The intensities of these spectra were normalized at the most intense band peak position.

TABLE 1: Observed Frequencies (ν_{obs}/cm^{-1}) and Bandwidths (fwhm/cm^{-1}) of $Al^+(CH_3OH)_n$ (n = 1−4) and $Al^+(CH_3OH)_n$−Ar (n = 1−3)

	$Al^+(CH_3OH)_n$		$Al^+(CH_3OH)_n$−Ar	
n	ν_{obs}/cm^{-1}	fwhm/cm^{-1}	ν_{obs}/cm^{-1}	fwhm/cm^{-1}
1	3490	130	3495	24
2	3580	90	3567	25
			3593	17
3	3594	50	3615	13
	3654	40	3630	10
	3000−3500	270	∼3300	
			∼3370	90
4	3663	60		
	<3200	150		
	3000−3500	260		

4. Results

IR photodissociation spectra of $Al^+(CH_3OH)_n$ (n = 1−4) are shown in Figure 1 (dashed lines), which were obtained by monitoring $Al^+(CH_3OH)_{n-1}$-ion yields formed by a loss of a methanol molecule. Observed frequencies (ν_{obs}) and full width at half-maximum (fwhm) are summarized in Table 1. For $Al^+(CH_3OH)_1$ and $Al^+(CH_3OH)_2$ clusters, relatively broad bands were observed at around 3500−3600 cm^{-1}, as seen in Figure 1a,b, whereas $Al^+(CH_3OH)_3$ and $Al^+(CH_3OH)_4$ ions have quite broad bands with more than 200 cm^{-1} fwhm in the region under 3500 cm^{-1} as well as sharp absorption bands above 3500 cm^{-1} (Figure 1c and d).

Solid lines in Figure 1 show IR photodissociation spectra of Ar-attached $Al^+(CH_3OH)_n$ (n = 1−3) clusters. Observed band widths in these spectra were considerably narrower than those of bare $Al^+(CH_3OH)_n$ due to the reduced internal energies in the Ar-attached cluster ions. For n = 1 and 2, a few sharp vibrational bands were observed in the energy region of 3500−3600 cm^{-1}, whereas one can find a band feature consisting of

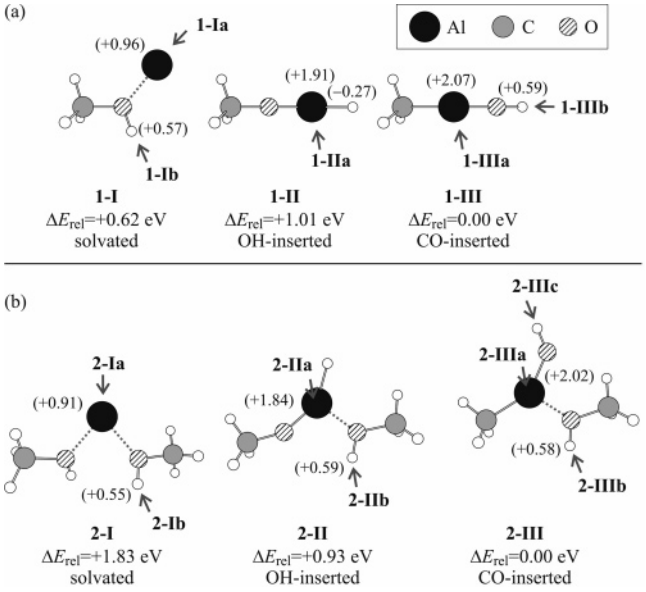

Figure 2. Optimized structures of (a) $Al^+(CH_3OH)_1$, solvated (**1-I**), OH-inserted (**1-II**), and CO-inserted (**1-III**) types, and (b) $Al^+(CH_3OH)_2$, solvated (**2-I**), OH-inserted (**2-II**), and CO-inserted (**2-III**) types, calculated at the B3LYP/6-31+G(d) level of theory. ΔE_{rel} shows the energy of each isomer in eV relative to the most stable isomer. Natural charges on Al and some H atoms are shown in parentheses. Gray arrows show Ar-atom binding sites, and neighboring notations (**1-Ia**, **1-Ib**, etc.) indicate isomers in which the Ar atom coordinates from the site denoted by the arrow. Dashed lines represent a direct bond to the Al^+ ion.

a few broad peaks in <3500 cm^{-1} as well as the two sharp ones above 3500 cm^{-1} for $n = 3$. Observed frequencies and widths of $Al^+(CH_3OH)_n-Ar$ ($n = 1-3$) are also summarized in Table 1.

5. Discussion: Theoretical Calculation and Assignment of the Cluster Structures

A. $Al^+(CH_3OH)_1$ and $Al^+(CH_3OH)_1-Ar$. In order to get information on the geometries of $Al^+(CH_3OH)_1$ and $Al^+(CH_3OH)_1-Ar$ ions, theoretical calculations of these ions were performed at the B3LYP/6-31+G(d) level of theory.[16] Optimized structures of $Al^+(CH_3OH)_1$ are shown in Figure 2a. There are three isomers for $Al^+(CH_3OH)_1$, as shown in the figure: solvated (**1-I**, C_s symmetry), OH-inserted (**1-II**, C_{3v} symmetry), and CO-inserted (**1-III**, C_{3v} symmetry) types. The solvated-type isomer, **1-I**, has a geometry where an Al^+ ion coordinates with a methanol molecule from the oxygen-atom side. Here the binding energy between Al^+ and CH_3OH was calculated to be 1.44 eV, which is almost the same as the value reported by Sodupe and Bauschlicher, 1.54 eV.[19] Among these, the CO-inserted type, **1-III**, was calculated to be the most stable isomer. The energy of each isomer relative to the most stable **1-III** isomer, ΔE_{rel}, is also shown in the figure.

Geometries of Ar-attached ions, $Al^+(CH_3OH)_1-Ar$, were also calculated at the same level of theory. Binding sites of the Ar atom at each isomer are shown by arrows in the figure. For **1-I**, there are two Ar-atom binding sites: one is the Al^+ ion and another is a hydrogen atom of the OH group of methanol. For the Ar-attached ions, a lower-case letter is added to the notations of the bare $Al^+(CH_3OH)_1$ ion to distinguish the binding sites of the Ar atom. The Ar atom in isomer **1-Ia** is located next to the Al^+ ion from the other side of the methanol molecule, whereas isomer **1-Ib** has a geometry in which the Ar atom binds with the hydrogen atom from the collinear direction with the O−H axis. The **1-Ib** isomer was calculated to be more stable

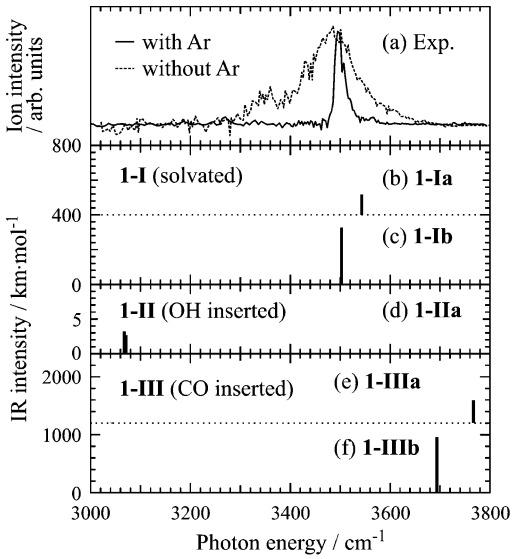

Figure 3. (a) Experimental IR photodissociation spectra of $Al^+(CH_3OH)_1$ with (solid line) and without (dashed line) an Ar atom, and (b−f) calculated vibrational spectra of $Al^+(CH_3OH)_1-Ar$ at the B3LYP/6-31+G(d) level with a scaling factor of 0.9654 for possible isomers.

than **1-Ia**. However, this result on the stability of $Al^+(CH_3OH)-Ar$ would include substantial error because the present B3LYP/6-31+G(d) calculation may be insufficient to estimate binding energies of Ar to $Al^+(CH_3OH)$. For **1-II**, only isomer **1-IIa** was calculated to be an equilibrium structure, where the Ar atom coordinates with the Al^+ ion in an almost perpendicular direction to the molecular axis. Isomer **1-III** was found to have two Ar-atom binding sites as well as isomer **1-I**: isomers **1-IIIa** and **1-IIIb**. The former is the same kind of isomer as **1-IIa**, that is, the Ar atom coordinates with the Al^+ ion from a perpendicular direction to the molecular axis. The latter has a geometry in which the Ar atom binds to an H atom of an OH group from a collinear direction with the O−H axis like **1-Ib**.

The harmonic vibrational frequencies of both $Al^+(CH_3OH)_1$ and $Al^+(CH_3OH)_1-Ar$ ions were also calculated at the B3LYP/6-31+G(d) level in order to assign observed bands in the IR photodissociation spectra and to determine the geometries of these ions. Calculated vibrational spectra are shown in Figure 3. Here, the inserted-type isomers may not be probed under the present experimental conditions because Al^+ produced by the loss of a methanol molecule was monitored for the bare $Al^+(CH_3OH)_1$ ion. The Al^+ ion can be produced by the three-body dissociation of isomers **1-II** and **1-III**: **1-II** $\rightarrow Al^+ + CH_3O + H$ and **1-III** $\rightarrow Al^+ + CH_3 + OH$. However, these fragmentation pathways are energetically impossible, even if the inserted-type isomers are produced in the cluster beam under the present conditions. Therefore, signals from the solvated-type **1-I** mainly contribute to the observed spectrum of $n = 1$ with an fwhm of 130 cm^{-1} (dashed line in Figure 1a). This broad bandwidth may be caused by IR multiphoton dissociation or dissociation of vibrationally excited ions because of the large Al^+-CH_3OH binding energy (1.44 eV), which corresponds to three IR photons in the OH stretching region. In contrast, signals from the inserted-type isomers can also be detected for the case of $Al^+(CH_3OH)_1-Ar$ because the loss of the Ar atom is monitored in the present measurement. Thus, we focus our attention on the results of the $Al^+(CH_3OH)_1-Ar$ ion in the rest of this section. In Figure 3, calculated vibrational spectra of **1-Ia** and **1-Ib** were found to well reproduce the experimental spectrum of $Al^+(CH_3OH)_1-Ar$. Calculated vibrational spectra of isomers **1-IIa**, **1-IIIa**, and **1-IIIb** hardly correspond to the

observed one. For example, **1-IIa** has no apparent peak around 3500 cm^{-1} because it has no OH functional group; the calculated peaks at 3068 and 3071 cm^{-1} for **1-IIa** correspond to CH stretching vibrations. In contrast, **1-IIIa** and **1-IIIb** show distinct peaks at 3767 and 3693 cm^{-1}, respectively. Thus, the most likely form of $Al^+(CH_3OH)_1-Ar$ contributing to the observed spectrum was not the most stable CO-inserted types, **1-IIIa** and **1-IIIb**, but the solvated-type isomers **1-Ia** and **1-Ib**. We cannot exclude the presence of the isomer **1-IIa**, because it may not be observed in the spectrum due to extremely low IR intensity. The inserted-type isomers may also be missed by the low concentration of the Ar-tagged ions in spite of the presence of the untagged species in the beam. A more detailed discussion on this insertion reaction is described in Section 5C.

B. $Al^+(CH_3OH)_n$ ($n = 2-4$) and $Al^+(CH_3OH)_n-Ar$ ($n =$ 2,3). Figure 2b shows optimized geometries of $Al^+(CH_3OH)_2$ calculated at the same level of theory as the $Al^+(CH_3OH)_1$ ions. There are at least three isomers of $Al^+(CH_3OH)_2$ as well as $Al^+(CH_3OH)_1$: solvated (**2-I**, C_2 symmetry), OH-inserted (**2-II**, C_1 symmetry), and CO-inserted (**2-III**, C_1 symmetry) types. These isomers have geometries in which the second methanol molecule coordinates with the each isomer of $Al^+(CH_3OH)_1$ (**1-I - 1-III**). For example, the second methanol binds with the Al^+ ion of **1-I** from the same side of the first methanol with a bond angle of $\angle O-Al^+-O = 81°$ in the solvated-type isomer **2-I**. An additional methanol also coordinates with the Al^+ ion of **1-II** and **1-III** in **2-II** and **2-III**, respectively. Among these, the most stable structure is the CO-inserted-type isomer, **2-III**. The Ar-atom binding site, indicated by arrows in the figure, is the Al^+ ion or the H atoms of OH groups, as already shown in the $Al^+(CH_3OH)_1$ ions. We discuss the $Al^+(CH_3OH)_2$ structure using the results on the Ar-attached ion as well as the $n = 1$ ion. Calculated vibrational spectra of the most stable structures in each type of isomer for the $Al^+(CH_3OH)_2-Ar$ ion are also shown in Figure 4 along with the experimentally obtained spectra. Only the spectrum of **2-Ib** can reproduce the experimental spectrum of $Al^+(CH_3OH)_2-Ar$, having sharp doublet peaks in the region of free OH stretching vibrations (see Table I in the Supporting Information for details on the calculated vibrational spectra). Therefore, **2-Ib** predominantly contributes to the dissociation spectrum. Although **2-III** has a characteristic vibration at an energy higher than 3700 cm^{-1}, no peaks were observed in this region of the experimental spectra (Figure 4a). For **2-II**, it has only one OH bond because the Al^+ ion inserts into an OH bond of the two methanol molecules. The vibrational frequency of the OH stretching mode of **2-IIb** was calculated to be slightly lower than the observed values. Therefore, **2-II** is less likely to be formed in the beam as well as **2-III**, although we cannot completely rule out the contribution of **2-IIb** because of insufficient accuracy of the calculated frequency. A discussion on the insertion reactions will be presented in the next section.

Optimized geometries and calculated vibrational spectra of $Al^+(CH_3OH)_3$ are shown in Figures 5 and 6, respectively. Seven isomers were obtained as equilibrium structures for the ion. Among these, two isomers, **3-I(3 + 0)** and **3-I(2 + 1)**, are classified as solvated-type isomers, whereas the remaining five isomers are inserted types: **3-II(3 + 0)** and **3-II(2 + 1)** are OH-inserted, and **3-III(3 + 0)**, **3-III(2 + 1)**, and **3-III(2 + 1)′** are CO-inserted-type structures. Arabic numbers in the parentheses of the notation indicate the numbers of methanol molecules coordinating with the Al^+ ion directly (the first number) and those solvating to the other methanol molecules (the second number). For example, all methanol molecules

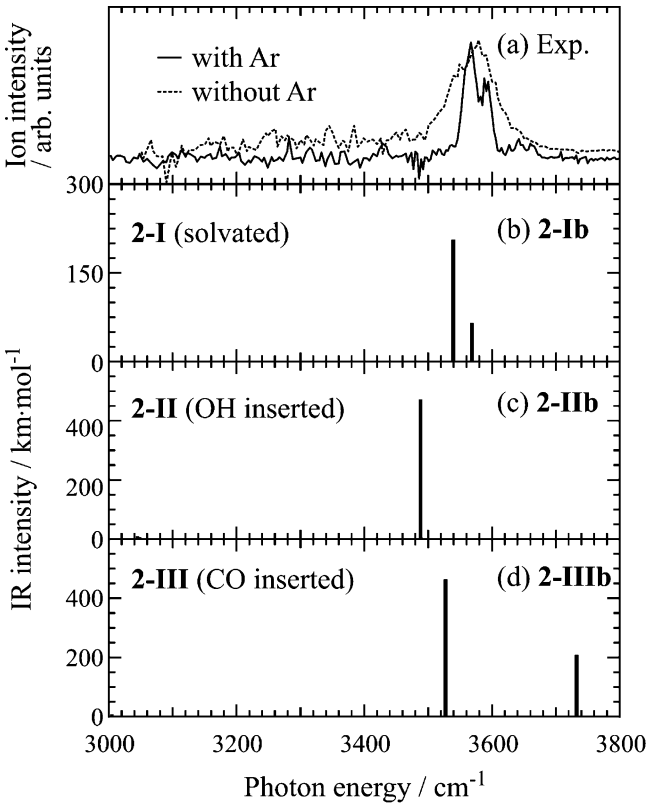

Figure 4. (a) Experimental IR photodissociation spectra of $Al^+(CH_3OH)_2$ with (solid line) and without (dashed line) an Ar atom, and (b−d) vibrational spectra of the most stable structures in each type of isomers for $Al^+(CH_3OH)_2-Ar$ calculated at the B3LYP/6-31+G(d) level with a scaling factor of 0.9654.

directly solvate to the Al^+ ion in **3-I(3 + 0)**, whereas the third methanol binds with other methanol molecules by two hydrogen bonds in **3-I(2 + 1)**. The latter isomer has a geometry in which an additional methanol forms two hydrogen bonds with the H atoms of the OH functional groups in **2-I**, forming a six-membered ring. For the OH-inserted-type isomers, the third methanol coordinates with the Al^+ ion of **2-II** in **3-II(3 + 0)**, and it binds with the H atom of the OH group of **2-II** in **3-II(2 + 1)**. In **3-III(3 + 0)**, the third methanol molecule binds with the Al^+ ion of the CO-inserted-type **2-III**, whereas the third methanol coordinates with the H atoms of the OH groups of **2-III** in **3-III(2 + 1)** and **3-III(2 + 1)′**. Among these seven isomers, **3-III(3 + 0)** was calculated to be the most stable, and energies of above isomers relative to **3-III(3 + 0)** (ΔE_{rel}) are also shown in Figure 5.

The results of the bare $Al^+(CH_3OH)_3$ ion are discussed here in detail, before we turn to the Ar-attached ion for $n = 3$. From the comparison of the experimental spectra with the calculated ones, **3-I(2 + 1)** (Figure 5c) was found to reproduce the observed band feature. The calculated spectrum of **3-III(2 + 1)′** is also partly in agreement with the observed spectrum, especially for the free OH stretching region (above 3500 cm^{-1}), although the hydrogen-bonded OH stretching of **3-III(2 + 1)′** (3183 cm^{-1}) was calculated to be lower than the observed band. Therefore, it is probable that CO-inserted-type **3-III(2 + 1)′** has a contribution to the experimentally obtained spectrum of the bare $Al^+(CH_3OH)_3$ ion. However, **3-III(2 + 1)′** is the most unstable isomer among the CO-inserted-type structures, as shown in Figure 5. Unstable isomers may have large contributions to the spectra because of their small binding energies. In the free OH stretching region, the double peaks observed in the spectrum for bare $Al^+(CH_3OH)_3$ cannot be explained only

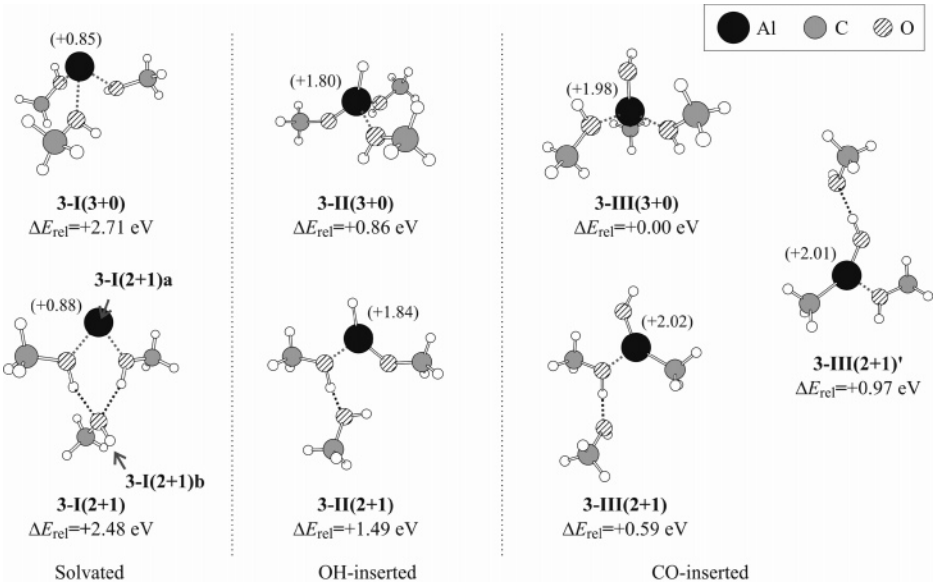

Figure 5. Optimized structures of $Al^+(CH_3OH)_3$, solvated (**3-I**), OH-inserted (**3-II**), and CO-inserted (**3-III**) types, calculated at the B3LYP/6-31+G(d) level of theory. Arabic numbers in the parentheses of the notation indicate the number of methanol molecules coordinating with the Al^+ ion directly (the first number) and solvating to the other methanol molecules (the second number). ΔE_{rel} shows the energy of each isomer in eV relative to the most stable structure. Natural charges on the Al atom are shown in parentheses. Gray and black dashed lines represent a direct bond to an Al^+ ion and a hydrogen bond to other methanol molecules, respectively. Gray arrows in **3-I(2 + 1)** represent Ar atom binding sites for the two isomers.

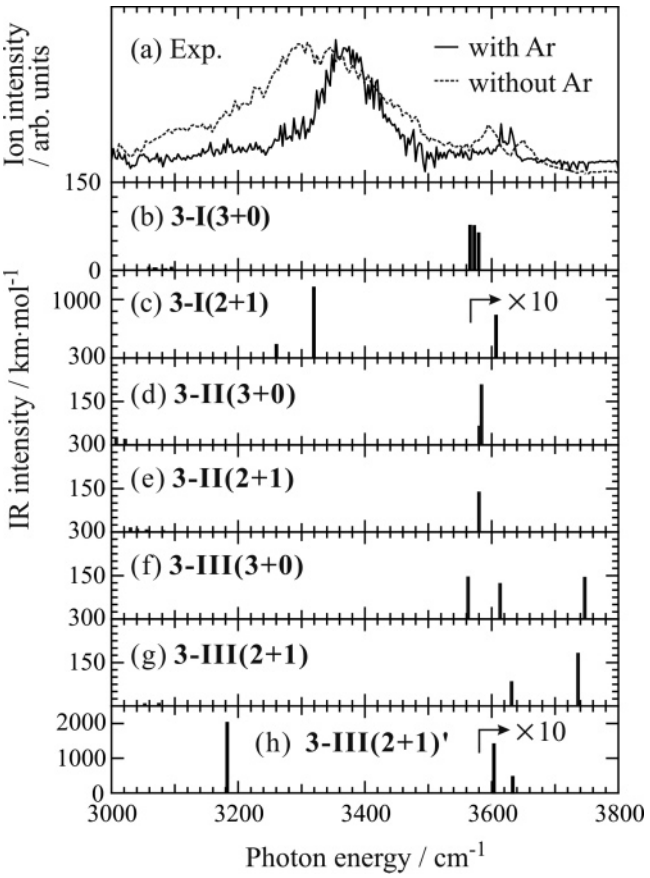

Figure 6. (a) Experimental IR photodissociation spectra of $Al^+(CH_3OH)_3$ with (solid line) and without (dashed line) an Ar atom, and (b−h) calculated vibrational spectra of $Al^+(CH_3OH)_3$ at the B3LYP/6-31+G(d) level with a scaling factor of 0.9654 for possible isomers.

by **3-I(2 + 1)**, because this isomer has one absorption band in this region. Other possible isomers, which may contribute to the spectrum having free OH stretching at ~3600 cm^{-1}, are **3-I(3 + 0)**, **3-II(3 + 0)**, and **3-II(2 + 1)** (Figure 6b,d,e). Thus we concluded that **3-I(2 + 1)** contributed to the experimental spectrum predominantly, and that there might be contributions of other isomers. However, we cannot proceed with further discussion on the bare $Al^+(CH_3OH)_3$ ion because of the broad bandwidths even in the free OH vibrations.

Now, let us discuss the result of the Ar-attached ion of **3-I(2 + 1)**, which is the most likely form for the bare $Al^+(CH_3OH)_3$ ion. Although other isomers noted above may have a contribution to the spectrum, here we focus our attention on the main species, **3-I(2 + 1)**. Geometries and vibrational frequencies of the Ar-attached ions, $Al^+(CH_3OH)_3-Ar$, were then calculated for **3-I(2 + 1)**. From this calculation, we found that there are two Ar-atom binding sites, as indicated by the gray arrows in Figure 5, which is consistent with the observed feature that two reproducible bands were observed in the free OH stretching vibration region. In other words, the doublet feature in the free OH stretching region may be attributed to the isomers where the Ar atom coordinates in the different environment. As a consequence, we concluded that, in the solvated-type isomer, the third methanol molecule is likely to bind with other methanols solvating to Al^+ without forming a direct bond with the metal ion.

For the $n = 4$ ion, only a spectrum of a nascent $Al^+(CH_3OH)_4$ ion could be measured because the intensity of an $Al^+(CH_3OH)_4-Ar$ ion was too small. Optimized structures and vibrational spectra of the $Al^+(CH_3OH)_4$ ion are shown in Figures 7 and 8, respectively. Geometry optimization of the $n = 4$ ion was performed only for the solvated-type isomers because observed features in the spectrum can be well reproduced by the solvated types as noted below, and also because the characteristic band at above 3700 cm^{-1} for the CO-inserted types was hardly observed in the spectrum. For the OH-inserted types, it could be expected that the vibrational frequencies of OH stretching for the OH-inserted types are calculated in the same region as those for the solvated types by analogy with $n = 2$ and 3. Therefore, we did not calculate these isomers, because it is difficult to estimate a contribution of this type of isomer from only the spectra presented here as in the discussion

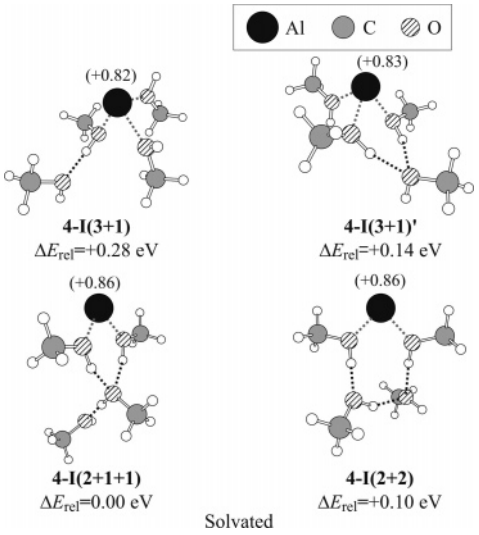

Figure 7. Optimized structures of the solvated-type isomers for $Al^+(CH_3OH)_4$ calculated at the B3LYP/6-31+G(d) level of theory. Arabic numbers in the parentheses of the notation indicate the number of methanol molecules coordinating with the Al^+ ion directly (the first number) and solvating to the other methanol molecules in the first and second layer (the second and third numbers). ΔE_{rel} shows the energy of each isomer in eV relative to the most stable structure. Natural charges on the Al atom are shown in parentheses. Gray and black dashed lines represent a direct bond to an Al^+ ion and a hydrogen bond to other methanol molecules, respectively.

about $n = 3$. Four isomers of the $Al^+(CH_3OH)_4$ ion were calculated as equilibrium structures. Isomers **4-I(3 + 1)** and **4-I(3 + 1)′** have an ion core of **3-I(3 + 0)**, in which the fourth methanol binds to the methanol molecule(s) of **3-I(3 + 0)** with one or two hydrogen bonds. On the other hand, **4-I(2 + 1 + 1)** and **4-I(2 + 2)** have the same geometry of ion cores with **3-I(2 + 1)** and **2-I**, respectively. The fourth methanol molecule in **4-I(2 + 1 + 1)** forms a hydrogen bond with a methanol in the second solvation layer of **3-I(2 + 1)**, whereas **4-I(2 + 2)** has a ring structure of four methanol molecules and the Al^+ ion. Among these solvated-type isomers, **4-I(2 + 1 + 1)** was found to be the most stable structure, as shown in Figure 7. In the vibrational spectra of these isomers shown in Figure 8, the spectrum of **4-I(2 + 1 + 1)** (Figure 8d) shows good agreement with the experimental spectrum, although the relative intensity of the observed spectrum is somewhat different from the calculated one. Thus, the most likely isomeric geometry contributing to the observed spectrum would be **4-I(2 + 1 + 1)**.

C. Insertion Reaction. The insertion reaction, which was reported already for the $Al^+(H_2O)_n$ ion by Inokuchi et al.,[12] is discussed in this section. As noted in the introduction, the stability of an isomer determines whether the insertion reaction occurs in the $Al^+(H_2O)_n$ system, as the barrier to insertion is low. In the present Al^+-CH_3OH clusters, we could not completely rule out the possibility of the insertion reaction into the OH bond from the IR photodissociation spectra, as noted above. On the other hand, we did not obtain positive results for the insertion reaction into the CO bond: no apparent signals from the CO-inserted isomers, which were the most stable isomers in all sizes examined, were observed in the spectra. One possible explanation of this result is that the potential energy barriers between inserted-type isomers and the solvated isomers are more important than the stability of the isomers. Potential energy barriers between **1-I** and **1-II** and between **1-I** and **1-III** were then calculated at the B3LYP/6-31+G(d) level of theory, although the accuracy of this calculation may be insufficient as

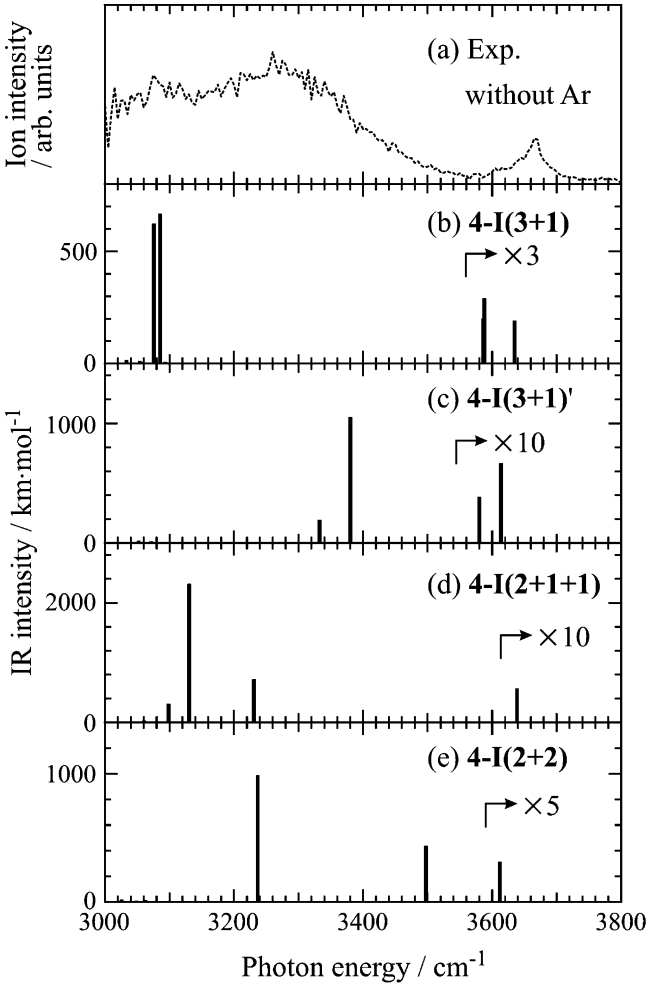

Figure 8. (a) Experimental IR photodissociation spectra of $Al^+(CH_3OH)_4$ without an Ar atom, and (b−e) calculated vibrational spectra of $Al^+(CH_3OH)_4$ at the B3LYP/6-31+G(d) level with a scaling factor of 0.9654 for possible isomers.

mentioned above. Figure 9 shows an energy diagram of the $Al^+(CH_3OH)_1$ system including predicted geometries of the transition states (TSs) for the insertion reactions. For the insertion reaction into the OH bond, the potential energy barrier was calculated to be 0.91 eV, which is larger than the total energy of the reactants, the Al^+ ion and the methanol molecule. Therefore, it is difficult to form **1-II** from the reaction between Al^+ and CH_3OH. The insertion reaction to form **1-III** was found to proceed with at least two steps: a rotation of a methyl group is necessary to form **1-III** from **1-I** in addition to the insertion reaction of the Al^+ ion into the CO bond, although these two steps, TS2 and TS2′, could not be connected directly as shown by the dotted line in the figure. As shown in Figure 9, there is an energy barrier of at least 0.37 eV for the reaction. This value is also larger than the total energy of the reactants, as noted above. Therefore, it is expected that both insertion reactions are less likely to proceed at $n = 1$ from these calculations.

Although there is no information on the potential barriers for the $n \geq 2$ ions and for the $Al^+(H_2O)_n$ ions at present, one possible explanation of the difference between the methanol and water systems is that the barriers of $Al^+(CH_3OH)_n$ are larger than those of $Al^+(H_2O)_n$, and thus $Al^+(CH_3OH)_n$ ions cannot overcome the potential energy barriers to form the inserted-type isomers. In general, the potential barrier is also expected to decrease dramatically with increasing cluster size n by the solvation effect. However, the present results imply that the barriers at $n = 2-4$ are still too high to allow the insertion

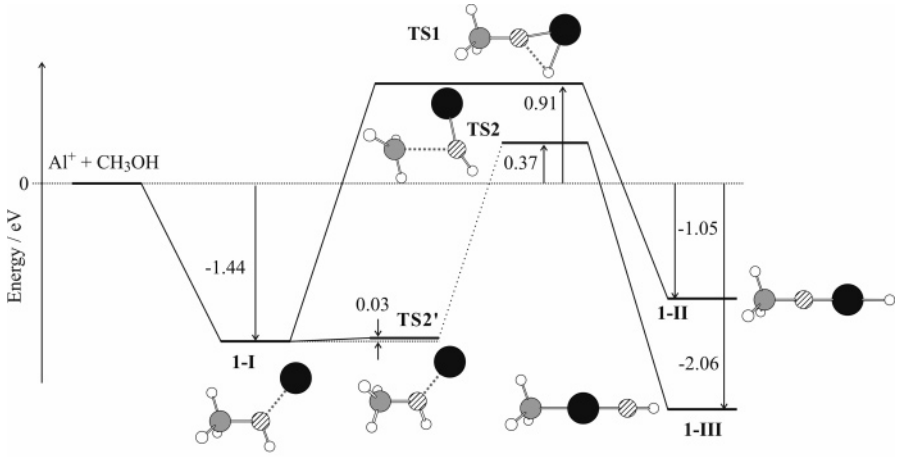

Figure 9. Potential energy barriers in eV and geometries of TSs between **1-I** and **1-II** and between **1-I** and **1-III** calculated at the B3LYP/6-31+G(d) level.

reactions to proceed. The insertion reaction of a metal cation into a CO bond in $V^+(CO_2)_n$ was reported to begin at a cluster size of $n = 9$.[20] However, the inserted product in a 1:1 complex, $OVCO^+$, was calculated to be more stable than the solvated-type $V^+(CO_2)$. This difference between experiment and theory was also explained by the activation energy between reactants and products as discussed here.

6. Conclusion

IR photodissociation spectra of cluster ions containing an Al^+ ion and methanol molecules $Al^+(CH_3OH)_n$ ($n = 1-4$) have been measured to examine the solvation structures and the possibility of intracluster reactions. In addition, spectra of Ar-attached cluster ions, $Al^+(CH_3OH)_n-Ar$ ($n = 1-3$), have been measured in order to get detailed information and also enhance the dissociation probability. In the spectra of $n = 1$ and 2 ions, sharp absorption bands were observed in the range of 3500−3600 cm^{-1}. The experimentally obtained spectra were found to be well reproduced by the spectra calculated for clusters classified as solvated-type isomers with no hydrogen bond. On the other hand, broad and intense bands were observed in the region of 3000−3500 cm^{-1} for $n = 3$ and 4, in addition to sharp peaks of free OH stretching vibrations. These red-shifted bands show the existence of hydrogen bonds in the clusters. Thus, the third and fourth methanol molecules do not have a direct bond with Al^+ but have hydrogen bonds with methanol molecules in the first solvation layer. From the consideration based on the results of theoretical calculations, it was found that the third methanol molecule has two hydrogen bonds with the first and second methanol molecules in $n = 3$, and that the fourth methanol molecule binds with the third methanol in $n = 4$. Furthermore, the intracluster insertion reaction reported in the $Al^+(H_2O)_n$ system was discussed from the standpoint of potential energy barriers as well as the stability of cluster ions. In the $Al^+(CH_3OH)_n$ cluster ions, no evidence of the insertion reaction was obtained in the present study, although the inserted-type isomers were calculated to be more stable than the solvated-type isomers at $n = 1-3$. The potential energy barriers to lead inserted-type isomers were calculated to be 0.37−0.91 eV for $n = 1$. One possible explanation of the difference between the methanol and water systems is that the barriers in the $Al^+(CH_3OH)_n$ system are larger than those in $Al^+(H_2O)_n$. Therefore, $Al^+(CH_3OH)_n$ ions may not overcome the potential energy barriers to form the inserted-type isomers, although information on the potential barriers is available for neither $n \geq 2$ ions nor the $Al^+(H_2O)_n$ ions at present.

Acknowledgment. This work was supported by the Joint Studies Program (2004) of the Institute for Molecular Science. A part of this work was also supported by the "Nanotechnology Support Project" and a Grant-in-Aid for Scientific Research of the Ministry of Education, Culture, Sports, Science and Technology (MEXT), Japan. The computations were performed using the Research Center for Computational Science, Okazaki, Japan. A.F. is supported by a Research Fellowship of the Japan Society for the Promotion of Science for Young Scientists.

Supporting Information Available: Scaled harmonic frequencies and IR intensities of isomers considered for $Al^+(CH_3OH)_n$ ($n = 1-4$) and $Al^+(CH_3OH)_n-Ar$ ($n = 1-3$). This material is available free of charge via the Internet at http://pubs.acs.org.

References and Notes

(1) Okumura, M.; Yeh, L. I.; Myers, J. D.; Lee, Y. T. *J. Chem. Phys.* **1986**, *85*, 2328.
(2) Chang, H.-C.; Wu, C.-C.; Kuo, J.-L. *Int. Rev. Phys. Chem.* **2005**, *24*, 553.
(3) Robertson, W. H.; Diken, E. G.; Price, E. A.; Shin, J.-W.; Johnson, M. A. *Science* **2003**, *299*, 1367.
(4) Headrick, J. M.; Diken, E. G.; Walters, R. S.; Hammer, N. I.; Christie, R. A.; Cui, J.; Myshakin, E. M.; Duncan, M. A.; Johnson, M. A.; Jordan, K. D. *Science* **2005**, *308*, 1765.
(5) Miyazaki, M.; Fujii, A.; Ebata, T.; Mikami, N. *Science* **2004**, *304*, 1134.
(6) Fielicke, A.; Kirilyuk, A.; Ratsch, C.; Behler, J.; Scheffler, M.; von Helden, G.; Meijer, G. *Phys. Rev. Lett.* **2004**, *93*, 023401.
(7) Lisy, J. M. *Int. Rev. Phys. Chem.* **1997**, *16*, 267.
(8) Duncan, M. A. *Int. Rev. Phys. Chem.* **2003**, *22*, 407.
(9) Walker, N. R.; Walters, R. S.; Duncan, M. A. *New J. Chem.* **2005**, *29*, 1495.
(10) Oepts, D.; van der Meer, A. F. G.; van Amersfoort, P. W. *Infrared Phys. Technol.* **1995**, *36*, 297.
(11) Walters, R. S.; Jaeger, T. D.; Duncan, M. A. *J. Phys. Chem. A* **2002**, *106*, 10482.
(12) Inokuchi, Y.; Ohshimo, K.; Misaizu, F.; Nishi, N. *Chem. Phys. Lett.* **2004**, *390*, 140.
(13) Watanabe, H.; Iwata, S. *J. Phys. Chem.* **1996**, *100*, 3377.
(14) Mune, Y.; Ohashi, K.; Ino, T.; Inokuchi, Y.; Judai, K.; Nishi, N.; Sekiya, H. *Chem. Phys. Lett.* **2006**, *419*, 201.
(15) Bullert, D.; Breckenridge, W. H. *Chem. Rev.* **2002**, *102*, 1595.
(16) Becke, A. D. *J. Chem. Phys.* **1993**, *98*, 5648.
(17) Frisch, M. J.; Trucks, G. W.; Schlegel, H. B.; Scuseria, G. E.; Robb, M. A.; Cheeseman, J. R.; Montgomery, J. A., Jr.; Vreven, T.; Kudin, K. N.; Burant, J. C.; Millam, J. M.; Iyengar, S. S.; Tomasi, J.; Barone, V.; Mennucci, B.; Cossi, M.; Scalmani, G.; Rega, N. Petersson, G. A.; Nakatsuji, H.; Hada, M.; Ehara, M.; Toyota, K.; Fukuda, R.; Hasegawa, J.; Ishida, M.; Nakajima, T.; Honda, Y.; Kitao, O.; Nakai, H.; Klene, M.; Li, X.; Knox, J. E.; Hratchian, H. P.; Cross, J. B.; Adamo, C.; Jaramillo, J.; Gomperts, R.; Stratmann, R. E.; Yazyev, O.; Austin, A. J.; Cammi, R.; Pomelli, C.; Ochterski, J. W.; Ayala, P. Y.; Morokuma, K.; Voth, G. A.; Salvador, P.;

Dannenberg, J. J.; Zakrzewski, V. G.; Dapprich, S.; Daniels, A. D.; Strain, M. C.; Farkas, O.; Malick, D. K.; Rabuck, A. D.; Raghavachari, K.; Foresman, J. B.; Ortiz, J. V.; Cui, Q.; Baboul, A. G.; Clifford, S.; Cioslowski, J.; Stefanov, B. B.; Liu, G.; Liashenko, A.; Piskorz, P.; Komaromi, I.; Martin, R. L.; Fox, D. J.; Keith, T.; Al-Laham, M. A.; Peng, C. Y.; Nanayakkara, A.; Challacombe, M.; Gill, P. M. W.; Johnson, B.; Chen, W.; Wong, M. W.; Gonzalez, C.; Pople, J. A. *Gaussian 03*, revision C.02; Gaussian, Inc.: Wallingford, CT, 2004.

(18) Scaling factors determined from the ratio of the experimental and calculated frequencies of the constituent methanol molecule could not reproduce the observed spectra well. Thus we adopted a scaling factor of 0.9654, which was reported to well reproduce the observed spectra of $Mg^+(H_2O)_n$ and $Al^+(H_2O)_n$ [ref 12].

(19) Sodupe, M.; Bauschlicher, C. W. *Chem. Phys. Lett.* **1991**, *181*, 321.

(20) Walker, N. R.; Walters, R. S.; Duncan, M. A. *J. Chem. Phys.* **2004**, *120*, 10037.